RevMexAA (Serie de Conferencias), **9**, 32–39 (2000)

CORONAL DIAGNOSTICS

J. C. Raymond and K. Wood

Harvard-Smithsonian Center for Astrophysics, Cambridge, MA, USA

RESUMEN

Los cocientes de líneas de emisión en el UV han permitido diagnosticar la densidad, temperatura, abundancias de elementos y el estado de ionización de los plasmas astrofísicos. Con la nueva generación de satélites de rayos-X, estas técnicas podrán usarse en los espectros de rayos-X. Es importante recordar que los cocientes proveen valores promediados a lo largo de la línea de visión y diferentes diagnósticos darán valores pesados de forma diferente. Existen varias suposiciones implícitas en los análisis de estos cocientes. En particular, se suele suponer que la profundidad óptica es despreciable. Damos algunos ejemplos de las bondades de usar la dispersión de fotones como una nueva herramienta de diagnóstico, ilustrando los peligros de usar los métodos usuales cuando la opacidad es alta.

ABSTRACT

Ultraviolet emission line ratios have long provided powerful diagnostics for the density, temperature, elemental abundances and ionization state of astrophysical plasmas. With the current generation of X-ray satellites, these techniques can be applied to X-ray spectra. It is important to remember that any such line ratio provides an average value along the line of sight, and different diagnostics will provide differently weighted averages.

Several assumptions are often made implicitly when emission line ratios are analysed. In particular, the optical depth is generally assumed to be negligible. This paper considers some examples of the opportunities provided by photon scattering for new diagnostic tools, and it considers the dangers of applying the standard methods when the optical depth is significant.

Key Words: **STARS: CORONAE — SUN: CORONA — TECHNIQUES: SPECTROSCOPIC — ULTRAVIOLET: STARS — X-RAYS: STARS**

Astrophysical Plasmas: Codes, Models, and Observations (Mexico City, 25-29 October 1999)
Editors: Jane Arthur, Nancy Brickhouse, & José Franco

1. INTRODUCTION

The intensity of an optically thin spectral line is given by the integral of its emissivity along the line of sight

$$\int N_{elem} f_{ion} A_{ji} N_j \, dx \quad , \tag{1}$$

where f_{ion} is the fraction of the element in the relevant ionization state, N_j is the population of the upper level, and A_{ji} is the radiative decay rate. The intensity ratio of two lines is the ratio of two such integrals, and it therefore contains elemental abundance, ionization state and, through the excitation rates which determine N_j, the electron temperature. The trick is to choose a line ratio which isolates an important physical parameter, such as electron density or temperature. The ratio then gives an average value for the parameter along the line of sight. It is important to remember that different diagnostic ratios will give differently weighted averages, for instance averages weighted with difference powers of the density.

In the following sections, we briefly summarize the classic density and temperature diagnostic line ratios. We then consider one of the complications often ignored, resonant scattering. In some cases, it is possible to use photon scattering to provide new diagnostics. They can be valuable simply because they involve lines which

Astrophysical Plasmas: Codes, Models, and Observations (Mexico City, 25-29 October 1999)
Editors: Jane Arthur, Nancy Brickhouse, & José Franco

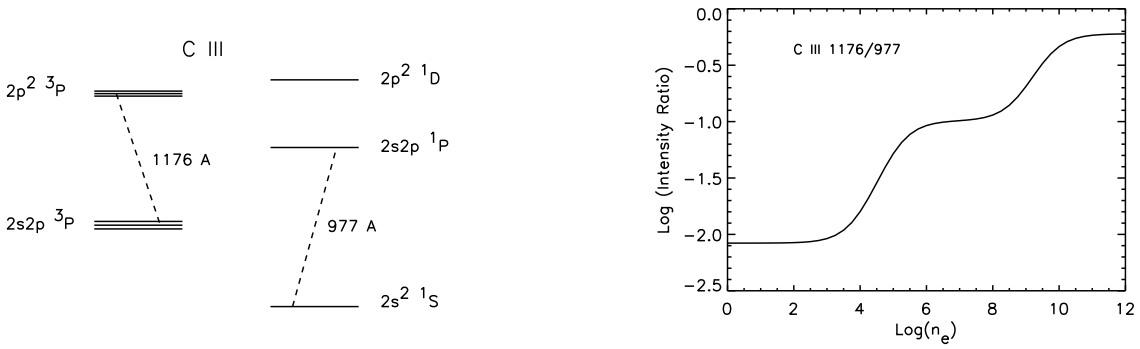

Fig. 1. (*Left*) Schematic energy level diagram for the Be-like ion C III. (*Right*) Intensity ratio of the λ1176 multiplet to the λ977 line.

are conveniently observed, but they may also provide unique information. Comparison of differently weighted averages can at least in principle be used to infer variations in the weighting factors along the line of sight.

1.1. *Density Diagnostics*

Among the most useful diagnostic intensity ratios are those for electron density. In general, one line is chosen whose intensity depends on the population of a metastable level, while the intensity of the other line does not. The population of the metastable level relative to the other levels undergoes a transition near a critical density at which the radiative decay rate equals the collisional de-excitation rate, $n_c = A_m/q_m$, where A_m and q_m are the total radiative and collisional rate coefficients out of the metastable level. The ratio is most useful near this critical density. It generally tends to a low density limit at lower densities, and at higher densities it either goes to a high density limit or one line becomes too weak to measure.

A convenient example is given by the beryllium-like ion C III. Figure 1 shows an energy level diagram approximately to scale. The $2s2p\ ^3P$ level contains 3 fine structure states, $^3\mathrm{P}_0$,$^3\mathrm{P}_1$ and $^3\mathrm{P}_2$, of which the $^3\mathrm{P}_1$ and $^3\mathrm{P}_2$ states have non-zero radiative decay rates. With electron collision rates from Berrington et al. (1985), this gives two critical densities near 10^5 and 10^9 cm^{-3}. Proton collisions (Ryans et al. 1998) significantly reduce the critical densities. Figure 1 also shows the behavior of the intensity ratio of the 1176 Å multiplet to the 977 Å resonance line as a function of density as computed with the CHIANTI package (Dere et al. 1997). The line ratio was computed for a temperature of 7×10^4 K, where the C III concentration peaks in ionization equilibrium. The line ratio contains a Boltzmann factor $\mathrm{e}^{-50{,}000/\mathrm{T}}$ through the energy dependence of the excitation rates to the $2s2p\ ^1P$ and $2p^2\ ^3P$ levels. This shifts the entire curve up or down for different temperatures. The curve shows two transitions from one plateau to another. The transition near 10^5 cm^{-3} corresponds to the critical density for the $2s2p\ ^3P_2$ state, which has only a forbidden transition to the ground state (A = 0.0047 s^{-1}; calculation by P. R. Young used in CHIANTI), while the transition near 10^9 cm^{-3} corresponds to the critical density for the $2s2p\ ^3P_1$ state, which has an intercombination decay to the ground state (A = 97 s^{-1}). Thus the line ratio is a useful diagnostic in the two density ranges near the two critical densities, though the 1176 Å multiplet may be difficult to measure due to its faintness in the lower density range.

As an example of a different type of density dependence, we consider another Be-like ion, O V, whose energy level diagram is sketched in Figure 2. Figure 2 also shows the intensity ratio of the lines from the $2s2p\ ^3P_2$ (forbidden decay) and $2s2p\ ^3P_1$ (intercombination decay) states as computed with CHIANTI (A values from P. R. Young, collision strengths from Zhang & Sampson 1992). This line ratio has a linear density dependence over a wide density range, but the 1213 Å line is generally too faint to be detectable at high densities, so again the ratio is most useful at densities near the critical density for the $2s2p\ ^3P_2$ state.

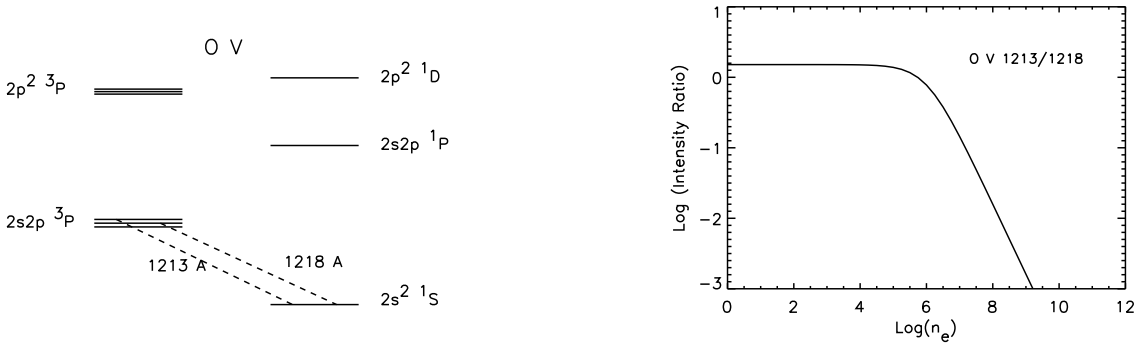

Fig. 2. (*Left*) Schematic energy level diagram for the Be-like ion O V. (*Right*) Intensity ratio of the $2s2p\ ^3P_2$ line to the $2s2p\ ^3P_1$ as a function of density.

This line ratio has been used by Pinfield et al. (1998) to find an electron density in the transition region of the quiet Sun. Their result was lower than the canonical quiet Sun transition region density, possibly due to the different weighting of the [O V]/O V] ratio diagnostic. Akmal et al. (1999) used the O V ratio to determine the electron density in a Coronal Mass Ejection from *SOHO*/UVCS observations at 3.5 solar radii. Comparison with the electron column density from *SOHO*/LASCO provided a means for measuring the geometrical thickness of the CME structure, and the density itself is a critical parameter for evaluating the heating and cooling rates of the CME plasma.

1.2. *Temperature Diagnostics*

Temperatures of astrophysical plasmas can be estimated a number of ways. In some cases the line width provides an upper limit on the kinetic temperature of the emitting ions, but bulk motions often make this a rather loose limit. Often the plasma is assumed to be in ionization equilibrium, so that the presence of an ion is taken as an indication that the emitting region contains some plasma near the temperature where the concentration of that ion peaks. If enough different lines are observed, a differential emission measure analysis gives the temperature range. Some error is introduced by the uncertainties in the ionization balance calculations, even if the assumption of ionization equilibrium is valid.

A more direct means for estimating the electron temperature is to use the intensity ratio of two lines of the same ion whose excitation threshold energies differ. The temperature dependence is then

$$\frac{I_1}{I_2} \quad \propto \quad e^{-E_1/kT+E_2/kT} \quad . \tag{2}$$

Ideally, the energy difference is comparable to kT. If the energy difference is smaller, the temperature dependence is weak. If the energy separation is much larger, the higher excitation line will be so faint that it is difficult to measure. Ideally, one can choose a line ratio which has no dependence on density and no significant contribution from recombination to either line. The difficulty is that strong spectral lines having very different excitation potentials are generally found at very different wavelengths, so that few promising pairs of lines are available within the spectral range of any one instrument. To compare the $3d \rightarrow 2s$ line of O VI at 173 Å with the $2p \rightarrow 2s$ doublet at 1034 Å, David et al. (1998) combined *SOHO*/CDS measurements with *SOHO*/SUMER observations. The calibration uncertainties of both instruments enter the analysis unless one considers only the relative temperatures of different solar regions, but David et al. were able to determine the electron temperature gradient in coronal holes.

An example of a line pair observable with a single instrument, and for that matter a pair at nearby wavelengths so that radiometric calibration is not an issue at all, is provided by another Be-like ion, Mg IX.

Astrophysical Plasmas: Codes, Models, and Observations (Mexico City, 25-29 October 1999)
Editors: Jane Arthur, Nancy Brickhouse, & José Franco

Astrophysical Plasmas: Codes, Models, and Observations (Mexico City, 25-29 October 1999)
Editors: Jane Arthur, Nancy Brickhouse, & José Franco

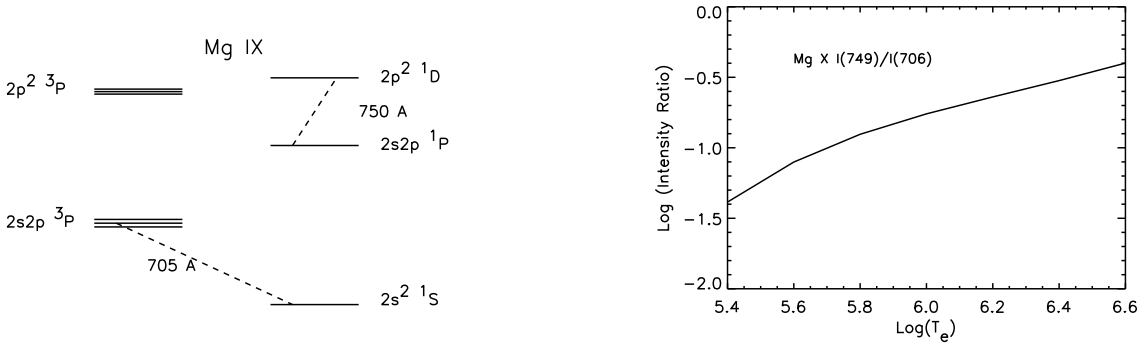

Fig. 3. (*Left*) Schematic energy level diagram for the Be-like ion Mg IX. (*Right*) Intensity ratio of the $2p^2\ ^1D_0 - 2s2p\ ^1P_1$ line to the $2s2p\ ^3P_1 - 2s^2\ ^1S_0$ as a function of temperature.

Wilhelm et al. (1998) used the ratio of the $2p^2\ ^1D_0 - 2s2p\ ^1P_1$ line at 749 Å to the $2s2p\ ^3P_1 - 2s^2\ ^1S_0$ line at 706 Å to determine temperatures in the solar corona from *SOHO*/SUMER spectra. They derived T_e significantly lower than has been found from *in situ* studies of the ionization state of the fast solar wind. The energy level diagram and the line ratio predicted by CHIANTI (P. R. Young A values, Keenan et al. 1986 collision strengths) are shown in Figure 3. This ratio depends on the population of the metastable $2s2p\ ^3P$ level, but at solar coronal densities this is in the low density limit.

The examples of temperature and density diagnostics were all chosen from the beryllium-like iso-electronic sequence to illustrate a point: One can choose a line ratio from an ion and find ranges of temperature and density where it depends mostly on temperature or mostly on density. While it is thus possible to isolate the two variables, it is important not to forget the other parameter entirely.

1.3. *Summary*

The diagnostic line ratios discussed above illustrate the standard line ratio technique that has been applied to astrophysical plasmas ranging from H II regions to solar flares for many decades. If suitable observations are available, these techniques are limited mainly by the accuracy of the atomic rates, and in fact these diagnostics have stimulated much important experimental and theoretical work to improve the atomic rates. An extensive review of these diagnostics is given by Mason & Monsignori-Fossi (1994).

2. OPTICAL DEPTH EFFECTS

A potentially serious caveat for the methods described above is that they assume that the plasma is optically thin. If one or both lines is optically thick in the emitting region or in the intervening line of sight, the interpretation can go awry. In some cases, one can correct for optical depth effects, but the correction may introduce large uncertainties. On the other hand, there are cases where the scattering itself can be used for diagnostic purposes.

The optical depth in a permitted line is given by

$$\tau \quad = \quad 0.026\ N_i\ f_{ij}/\delta\nu \quad , \tag{3}$$

where N_i is the column density in the lower level of the absorption line (cm^{-2}), f_{ij} is the oscillator strength and $\delta\nu$ is the width of the line in Hz. For line widths of order 25 km s^{-1}, typical of the non-thermal motions in the solar corona, cross sections are in the range of a few $\times 10^{-14}$ cm^2 for ultraviolet lines and a few $\times 10^{-15}$ cm^2 for X-ray lines. The product of elemental abundance and ion concentration is typically 10^{-4} to 10^{-5} for strong

lines, so that the stronger lines become optically thick at hydrogen column densities of order $10^{19} - 10^{21}$ cm^{-2}. The strongest emission lines are generally those which arise from the dominant ions (He-like or Ne-like) of the most abundant elements (C, O, Fe), and these are the most likely to reach significant optical depths. The O VII resonance line at 22 Å is used in density diagnostic ratios. Acton & Brown (1978) considered the effects of the long path lengths near the solar limb on the resonance line. The effects of scattering near the solar limb on the Fe IX and Fe XII lines that dominate the 171 and 195 Å bands of the *TRACE* satellite were studied by Schrijver & McMullen (1999). The coronal ion whose optical thickness has been most intensively studied is Fe XVII. The 15.01 Å resonance line is exceptionally bright, so it has been used to investigate elemental abundances in solar active regions. However, the ratio of this line to other Fe XVII lines having smaller oscillator strengths (15.26 Å, 17.10 Å) disagrees with theoretical predictions and laboratory measurements, and the discrepancy may result from scattering (e.g., Schmelz et al. 1997; Saba et al. 1999).

We consider first some examples of the use of scattering for diagnostic purposes, then turn to the more complicated issue of the influence of geometry on the intensities of strong lines.

Astrophysical Plasmas: Codes, Models, and Observations (Mexico City, 25-29 October 1999)
Editors: Jane Arthur, Nancy Brickhouse, & José Franco

2.1. *Coronal Densities*

The emissivity of a spectral line due to local excitation is given by the excitation rate coefficient and the electron and ion densities:

$$q_{ex}(T)\ n_e\ n_i\ . \tag{4}$$

The emission due to scattering of photons from an external source, on the other hand, is

$$I_\lambda\ \sigma_\lambda\ n_i\ \ . \tag{5}$$

Thus, if the excitation rate, q_e, scattering cross section, σ_λ, and illuminating flux, I_λ, are known, the ratio of the collisional contribution to the radiative contribution of a spectral line gives an average electron density. This is most reliable if the optical depth is small enough that finite optical depth can be ignored, but large enough that the scattered component is bright enough to observe. Like all the other diagnostics, the average is weighted, in this case mainly by the density of the ion. Differently weighted averages may give different, but still correct, results. In principle, comparison of differently weighted averages could yield novel information about gradients or clumping in the observed plasma.

This technique has been applied extensively to *SOHO*/UVCS observations of the solar corona. The easiest application is the O VI doublet at $\lambda\lambda$1032, 1037. The excitation rates of these lines are in a 2:1 ratio determined by the statistical weights, as are the scattering cross sections, and the illuminating fluxes in the two lines from the solar disk are also in a 2:1 ratio. Therefore, the locally excited component of the O VI lines are in a 2:1 ratio, while the scattered component has a 4:1 ratio. In one example, UVCS measured an O VI doublet ratio of 2.38:1 at 2 solar radii just before a Coronal Mass Ejection passed across the UVCS slit on June 11, 1998. Separation of the collisional and scattering components (and use of the collisional excitation rate and O VI intensities incident from the solar disk) leads to a density of 3.8×10^6 cm^{-3}. A Type II radio burst was observed at the same time, and assuming that the fundamental frequency of the radio emission is the plasma frequency, the inferred density is 7.5×10^6 cm^{-3} (Raymond et al. 1999). The difference between these densities might result from the averaging along the line of sight in the UVCS analysis, or it might result from compression in the Coronal Mass Ejection shock.

2.2. *Geometrical Effects*

The nature of the effects of scattering depends on the optical depth. For $\tau \simeq 1$, the only effect is to change the photon's direction. At somewhat higher optical depths, photons at one wavelength may be converted to entirely different spectral ranges. For instance, if a Lyβ λ1025 photon is absorbed by an H atom, it stands a 12% chance of being converted to an Hα photon, leaving the atom in the excited (metastable) 2s level. At low densities the atom will decay by emitting a 2-photon pair, while at higher densities a 2s-2p excitation will lead to a Lyα photon. In either case, the original Lyβ photon is destroyed, and optical depths $\tau \simeq 10$ lead to suppression of the Lyβ intensity and enhancement of Hα. This effect is important in the formation

of the Hα profiles of interstellar shock waves (e.g., Ghavamian 1999). At still higher optical depths, photons can be trapped long enough that collisional de-excitation will destroy them. At low τ, collisional de-excitation becomes important at a critical density A_{ji}/q_{ji}, which is of order 10^{15} cm^{-3} for LS allowed ultraviolet lines. Scattering effectively decreases A_{ji} by the escape probability, of order $1/\tau$.

For most coronal studies, we are interested in modest optical depths, so we will concentrate on the geometrical effects. If the emitting region is spherically symmetric, this has no effect at all on the emerging flux, though it can change the intensity distribution across the face of the sphere. If the emitting region is not spatially resolved, the line ratios are unchanged. If the emitting region is elongated in 1 or 2 dimensions, photons tend to be scattered away from those directions and emerge from the narrowest direction. Thus the intensity may be strongly reduced if one observes the emitting region end-on, or slightly enhanced if one views it face-on. If one observes an individual feature, such as an active region loop end-on, the effect can be substantial.

Figure 4 shows a Monte Carlo simulation of a coronal loop seen in the Fe XVII 15.01 Å line from different angles (K. Wood & J. C. Raymond 2000, in preparation). The code is based on that described by Code & Whitney (1995) as modified to run on a linear Cartesian grid (Wood & Reynolds 1999). It includes forced first scattering (Witt 1977) and a "peeling off" procedure (Yusef-Zadeh, Morris, & White 1984). The simulations used a Rosner, Tucker, & Vaiana (1978) coronal loop model for the density and temperature structure with $\log(T_{max}) = 6.8$ and a loop length 10^{10} cm. The Fe abundance was taken as a typical FIP-enhanced value of 3 times the photospheric abundance, and the emissivity was based upon the Arnaud & Raymond (1992) ionization equilibrium and the Smith et al. (1985) excitation rate. For this choice of T_{max}, the Fe XVII line is emitted more strongly from the legs of the loop than from the apex.

Each column shows the appearance of the loop as viewed from (top to bottom) directly above, 45° from vertical, face-on, rotated by 45°, and end-on. The left column is the appearance that an optically thin line would present. When seen from above, the loop is bright at the footpoints, but viewed end-on it is bright at the top, in both cases because of geometrical projection. Thus an appearance of emission concentrated at loop footpoints or at the top of the loop may result purely from projection at a given viewing angle. These models are similar to those of Alexander & Katsev (1996).

The middle column shows the appearance including the appropriate opacity for the Fe XVII 15.01 Å line. The optical depth drastically reduces the geometrical projection effects because the long path length that enhances the brightness of an optically thin line implies a large optical depth for an optically thick one. The loop is actually $\sim 20\%$ brighter when seen face-on because photons tend to scatter from the end-on toward the face-on directions. The total flux from the loop seen end-on is less than half the optically thin value.

The right column shows the effects of embedding the loop in a lower density region. The local emission from the diffuse region is faint because of the low density, but scattering of photons produced by the bright loop creates a halo in the diffuse region. Furthermore, attenuation in the diffuse plasma makes the far side of the loop fainter than the near side (right column, second panel from the bottom). Asymmetric loops are often observed in *SOHO*/EIT and *TRACE* images. Most are probably asymmetric in reality, but optical depth may play a role in some observed morphologies.

If one observes an ensemble of loops, for instance spread over the surface of another star, the effects tend to average out. Equal numbers of photons are scattered out of the line of sight and into it. A net effect may still arise if the emissivity and the opacity vary in different ways, however. Given the electron density factor in the emissivity and its absence in the opacity, such differences are likely. For instance, if the emission is dominated by dense, low-lying coronal loops and larger, lower density loops envelope them with significant opacity but little emissivity, there will be a tendency for photons to be scattered back down into the surface of the star. Models similar to those in the righthand column of Figure 4 can easily be constructed to reduce the intensities of lines having large oscillator strengths. They will undoubtedly be invoked when line ratio anomalies appear is *Chandra* or *XMM* data. Proving that optical depth is indeed the explanation for a given anomaly will undoubtably be a challenge.

This work was supported by NASA grants NAG-528 and NAG-6039 to the Smithsonian Astrophysical Observatory.

Astrophysical Plasmas: Codes, Models, and Observations (Mexico City, 25-29 October 1999)
Editors: Jane Arthur, Nancy Brickhouse, & José Franco

Astrophysical Plasmas: Codes, Models, and Observations (Mexico City, 25-29 October 1999)
Editors: Jane Arthur, Nancy Brickhouse, & José Franco

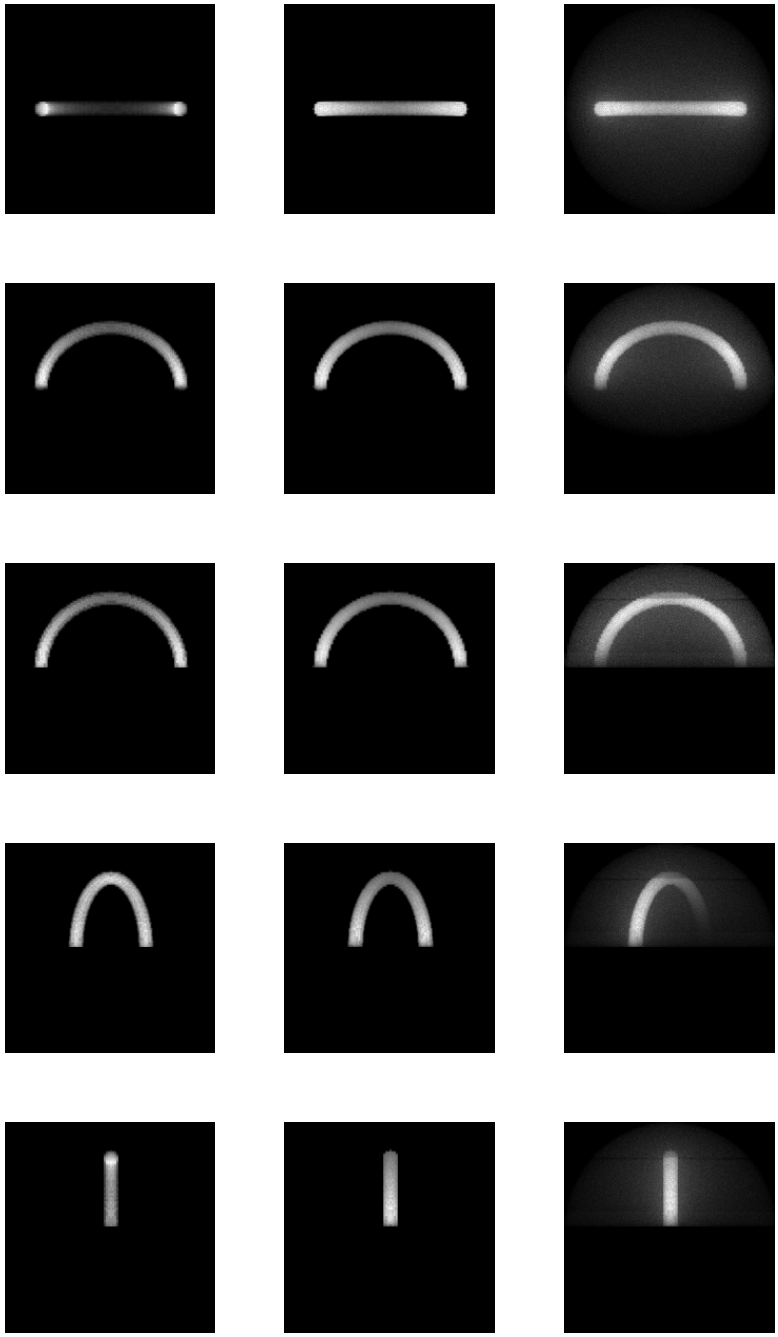

Fig. 4. Appearance of a coronal loop in the Fe XVII 15.01Å resonance line as simulated by K. Wood & J. C. Raymond (2000, in preparation). The left column assumes optically thin emission, the center column includes optical depth of the loop, and the right column embeds the loop in a lower density medium having faint emission but significant optical depth.

REFERENCES

Acton, L. W, & Brown, W. A. 1978, ApJ, 225, 1065
Akmal, A., Raymond, J., Vourlidas, A., & Thompson, B. 1999, Fall AGU Meeting
Alexander, D., & Katsev, S. 1996, Sol. Phys., 167, 153
Arnaud, M. A., & Raymond, J. C. 1992, ApJ, 398, 394
Berrington, K. A., Burke, P. G., Dufton, P. L., & Kingston, A. E. 1985, ADNDT, 33, 195
Code, A. D., & Whitney, B. A. 1995, ApJ, 441, 400
David, C., Gabriel, A. H., Bely-Dubau, F., Fludra, A., Lemaire, P., & Wilhelm, K. 1998, A&A, 336, 90
Dere, K. P., Landi, E., Mason, H. E., Monsignori Fossi, B. C., & Young, P. R. 1997, A&AS, 125, 149
Ghavamian, P. 1999, Ph.D. Thesis, Rice University
Keenan, F. P., Berrington, K. A., Burke, P. G., Dufton, P. L., & Kingston, A. E. 1986, Phys. Scripta, 34, 216
Mason, H. E., & Monsignori Fossi, B. C. 1994, A&A Rev., 6, 123
Pinfield, D. J., Mathioudakis, M., Keenan, F. P., Phillips, K. H. J., & Curdt, W. 1998, A&A, 340, L15.
Saba, J. L. R., Schmelz, J. T., Bhatia, A. K., & Stong, K. T. 1999, ApJ, 510, 1064
Schmelz, J. T., Saba, J. L. R., Chauvin, J. C., & Stong, K. T. 1997, ApJ, 477, 509
Schrijver, C. J., & McMullen, R. A. 1999, preprint
Raymond, J. C., Thompson, B. J., St. Cyr, O. C., Gopalswamy, N., Kahler, S., Kaiser, M., Lara, A., Ciaravella, A., Romoli, M., & O'Neal, R. 1999, GRL, in press
Rosner, R., Tucker, W. H., & Vaiana, G. S. 1978, ApJ, 220, 643
Ryans, R. S. I., Foster-Woods, V. J., Reid, R. H. G., Keenan, F. P., & Copeland, F. 1998, A&A, 336, 393
Smith, B. W., Raymond, J. C., Mann, J., & Cowan, R. D. 1985, ApJ, 298, 898
Wilhelm, K., Marsch, E., Dwivedi, B. N., Hassler, D. M., Lemaire, P., Gabriel, A. H., & Huber. M. C. E. 1998, ApJ, 500, 1023
Witt, A. N. 1977, ApJS, 35, 1
Wood, K., & Reynolds, R. J. 1999, ApJ, 525, 799
Yusef-Zadeh, F., Morris, M., & White, R. L. 1984, ApJ, 278, 186
Zhang, H. L., & Sampson, D. H. 1992, ADNDT, 52, 143

Astrophysical Plasmas: Codes, Models, and Observations (Mexico City, 25-29 October 1999)
Editors: Jane Arthur, Nancy Brickhouse, & José Franco

J. C. Raymond and K. Wood: Center for Astrophysics, 60 Garden St., Cambridge, MA 02138, USA (jraymond, kwood@cfa.harvard.edu).